Journal of Catalysis 392 (2020) 150–158

Contents lists available at ScienceDirect

Journal of Catalysis

journal homepage: www.elsevier.com/locate/jcat

Interplay between carbon dioxide enrichment and zinc oxide promotion of copper catalysts in methanol synthesis

Remco Dalebout, Nienke L. Visser, C.E. Lisette Pompe, Krijn P. de Jong, Petra E. de Jongh *

Inorganic Chemistry and Catalysis, Debye Institute for Nanomaterials Science, Utrecht University, Universiteitsweg 99, 3584 CG Utrecht, the Netherlands

ARTICLE INFO

Article history:
Received 9 July 2020
Revised 30 September 2020
Accepted 2 October 2020
Available online 15 October 2020

Keywords:
Methanol synthesis
Syngas composition
CO_2 conversion
Selectivity
ZnO_x promotion
Copper nanoparticles
Carbon support

ABSTRACT

Methanol synthesis over $Cu/ZnO/Al_2O_3$ is a key industrial reaction. Typically, a ZnO_x promoter and CO_2 enrichment of the feed are applied to maximize the syngas conversion. However, understanding the effects of these additives on the performance of the Cu catalysts is obscured by the strong interaction between the ZnO_x promoter and oxidic supports. Here, we use Cu nanoparticles on graphitic support to study the interplay between CO_2 concentration and ZnO_x promotion. CO_2 enrichment enhanced the activity with an optimum at 3 vol% in the feed, but only if the ZnO_x promoter was present, demonstrating the intricate interaction between the two. Interestingly, not only the activity but also the methanol selectivity was enhanced by CO_2 enrichment, and even further by the addition of ZnO_x. Understanding not only the role of the individual components, but also the interaction between them, is important to design catalysts for processes with more flexible feed compositions.

1. Introduction

Methanol is a key chemical building block for the production of a wide range of chemicals including formaldehyde, olefins, acetic acid, and dimethyl ether [1,2]. The annual methanol production is around 100 million tons and the demand increases with about 4–5% per year [1,3,4]. Typically, a CO_2-enriched synthesis gas feed ($H_2/CO/CO_2$) is passed over a $Cu/ZnO/Al_2O_3$ catalyst at elevated temperatures (473–573 K) and pressures (40–100 bar) [5,6]. Cu is the main active component in this catalyst, which is promoted by ZnO_x, whereas Al_2O_3 mainly serves for structural stability [7–10]. Other catalyst formulations such as Cu nanoparticles supported on ZrO_2 [11], GaO_x [9], CeO_x [12] or in the presence of Al, Ga, Mg, Mn, and/or Zr [13–15], $NiGa_x/SiO_2$ [16,17], $GaPd_2/SiO_2$ [18] and In_2O_3/ZrO_2 [19] have also been investigated.

Small amounts of CO_2 (2–6%) are generally added to the syngas mixture to increase the conversion of Cu-based methanol synthesis catalysts [20–23]. Although CO can be directly hydrogenated to methanol [21,23–27], it has been clearly documented that in CO_2-enriched feed streams the vast majority of the methanol molecules originates from the hydrogenation of CO_2 molecules [11,22,27,28]. The water formed in this process drives the water–gas shift (WGS) reaction ($CO + H_2O \rightarrow CO_2 + H_2$) [28,29] by reacting with CO in the feed over a Cu surface. In this way constant but low concentrations of water and CO_2 are sustained in the reaction atmosphere. Due to energy storage considerations it could be desirable to operate the process with high concentrations of CO_2 in the feed, or even with a pure H_2/CO_2 feed. However, hydrogenation of pure CO_2 results in relatively high water concentrations, which give rise to a poor catalyst stability [30]. Even though the redistribution of the ZnO_x promoter can also play a role, deactivation is mostly due to Cu particle growth, as investigated in detail in our lab [31–33] and by others [34–37]. Although the fact that slight CO_2 enrichment increases the catalyst activity and decreases its stability, it is not yet known how and if the promoter plays a role in this.

Likewise, the influence of ZnO_x on methanol synthesis is well known with a standard concentration of CO_2 in the feed [6,11,20–22,38,39], but little is understood about its influence in different CO_2 concentrations or while hydrogenating pure CO. Martin et al. [29] showed that for a Cu/Al_2O_3 catalyst the methanol formation rate increased by one order of magnitude upon ZnO_x promotion in the absence of CO_2 in the feed, while Nielsen et al. [25] reported no significant change in the activity between 50 wt % Cu/Al_2O_3 and $Cu/ZnO/Al_2O_3$ catalysts, whereas Studt et al. [27] and Zander et al. [40] even reported a poisoning effect by ZnO_x on the activity of a 86 wt% Cu/MgO catalyst. It hence seems that the effect of ZnO_x also depends on the type of oxidic support used. ZnO_x is known to have a relatively strong interaction with oxidic

* Corresponding author.
E-mail address: P.E.deJongh@uu.nl (P.E. de Jongh).

https://doi.org/10.1016/j.jcat.2020.10.006
0021-9517/

supports, which also depends on the reaction conditions [41–43]. As a result, a large fraction of the ZnO_x might not be in the form of zinc oxide, but rather present as for instance zinc aluminates or silicates. Hence, oxidic supports might hinder the understanding of the intrinsic influence of ZnO_x on the performance of Cu catalysts. Graphite-like materials as a non-oxidic support may limit these effects and has for example been used as a support for Cu(Zn)O_x particles in methanol synthesis [44], Ru particles in Fischer-Tropsch synthesis [45] and bimetallic CuNi in dimethyl carbonate synthesis [46].

A decisive factor in catalysis is the selectivity. Methanol synthesis from CO_2-containing syngas delivers a high selectivity, typically more than 98% [14,21,34,44,47–49]. This remarkably high selectivity is typically attributed to the limited effectiveness of Cu to dissociate CO, thereby limiting the production of the thermodynamically more stable hydrocarbons. Even though the methanol selectivity is generally high, it is still very relevant to investigate the nature of the side products, and how the product distribution is influenced by the ZnO_x promoter and the CO_2 concentration.

Here, we study the combined effect of different amounts of CO_2 (including its absence) to the syngas feed and ZnO_x promotion on the methanol selectivity and formation rate on carbon-supported Cu(Zn)O_x model catalysts, to obtain insights into how these factors affect the performance of methanol synthesis catalysts. We use graphitic carbon as a model support for Cu(Zn)O_x nanoparticles as this avoids strong metal-support interactions [42] and hence is expected to limit spectator species such as zinc mixed metal oxides.

2. Experimental

2.1. Chemicals

Copper nitrate ($Cu(NO_3)_2{\cdot}3H_2O$, Acros Organics, 99%), zinc nitrate ($Zn(NO_3)_2{\cdot}6H_2O$, Sigma Aldrich, ≥99%), high surface area graphite (TIMREX E-HSAG500 AF-246 B78, TIMCAL Graphite & Carbon) and nitric acid (HNO_3, Merck, 65%) were used as received. Reference was a commercial Cu/ZnO/Al_2O_3/MgO catalyst from Alfa Aesar, containing a Cu/Zn/Al/Mg ratio of 63.8/24.8/10.1/1.3 wt%. Silicon carbide (SiC, Alfa Aesar, ≥98.8%, 46 grit) was sieved in a 212–425 μm fraction, calcined at 1073 K for 10 h, subsequently washed with 65% HNO_3 and rinsed with water until pH 7 was reached, and finally dried at 393 K overnight before use.

2.2. Catalyst synthesis

Typically, *ca.* 2.3 g of carbonaceous support (high surface area graphite, Brunauer-Emmett-Teller (BET) surface area 509 $m^2\ g^{-1}$) was dried at approximately 443 K under dynamic vacuum for 1.5 h to remove water from the pores. After cooling down to room temperature the fine carbon powder was (co-)impregnated to incipient wetness [50], defined as 95% of the total pore volume by N_2 physisorption, under static vacuum with a 0.1 M HNO_3 solution containing copper (and zinc) nitrates. The concentration of copper (and zinc) nitrates were chosen such to obtain the desired weight loading. The impregnated support was dried at room temperature under dynamic vacuum overnight, and reduced at 503 K (ramp 2 K min^{-1}) in a 100 mL min^{-1} flow of 20% H_2/N_2 for 2.5 h. To be able to store and handle the catalyst in the oxidized state, it was exposed to a flow of 100 mL min^{-1} flow of 5% O_2/N_2 for 1 h, heated to 473 K with a ramp of 1 K min^{-1} and oxidized at 473 K in 15% O_2/N_2 for 1 h. The obtained *X*-Cu/C and *X*-$CuZnO_x$/C catalysts, in which *X* represents the surface-averaged CuO size in the fresh catalyst, had a theoretical Cu weight loading of *ca.* 8.1 ± 0.3 wt% and a ZnO loading of 0.1 or 5.3 wt%.

2.3. Catalyst characterization

2.3.1. N_2 physisorption

Physisorption was measured on a Micromeritics TriStar II Plus apparatus at 77 K. Prior to analysis the sample was dried at 443 K under a N_2 flow overnight. The BET surface area was determined according to the IUPAC procedure [51]. Pore size distributions were established *via* a Barrett-Joyner-Halenda (BJH) analysis, using a carbon black reference thickness curve with a Faas correction. The total pore volume V_{tot} was derived from the amount of N_2 adsorbed at p/p_0 = 0.995. The micropore volume V_{micro} was obtained *via* the *t*–plot method using a carbon black reference thickness curve ($t = 2.98 + 6.45{\cdot}(p/p_0) + 0.88{\cdot}(p/p_0)^2$) fitted in the linear N_2 monolayer adsorption regime. Finally, the mesopore volume V_{meso} was derived from integration of the adsorption-based BJH curve between 2 and 50 nm. Finally, the macropore volume V_{macro} was defined as the difference between the total pore volume and the sum of the t-plot micropore volume and BJH-derived mesopore volume.

2.3.2. EM imaging and EDX mapping

Catalysts were imaged by transmission electron microscopy (TEM) on a Thermo Scientific Talos F200X apparatus, operating at 200 kV and equipped with a high-brightness field emission gun (X-FEG) and Super-X™ energy-dispersive X-ray (EDX) detectors. To this end, holey carbon film-coated Cu or Au grids (Agar, 300 mesh) were dry-loaded with finely ground sample (<25 μm). Number-averaged CuO particle sizes (d_N) were determined by measuring at least 350 individual particles at different locations within the sample. These sizes were translated into surface-averaged (d_S) and volume-averaged (d_V) particle sizes, including the standard deviations in the width of the particle size distribution, *via* $d_S \pm s_S = \sqrt{\frac{1}{N}\sum_{i=1}^{N} d_i^2} \pm \sqrt{\frac{1}{N-1}\sum_{i=1}^{N}(d_i - d_S)^2}$ and $d_V \pm s_V = \sqrt[3]{\frac{1}{N}\sum_{i=1}^{N} d_i^3} \pm \sqrt{\frac{1}{N-1}\sum_{i=1}^{N}(d_i - d_V)^2}$, in which d_i indicates the diameter of the i-th particle and N represents the total number of measured particles.

Qualitative, chemical compositions were mapped by EDX spectroscopy, while imaging in high-angle, annular, dark-field, scanning transmission electron microscopy (HAADF-STEM) mode. The elemental maps were acquired using Velox™ analytical imaging software. The acquisition time per EDX map was at least 15 min, and the probe current was around 700 pA.

2.3.3. XRD analysis

Powder X-ray diffractograms were recorded at a Bruker AXS D2 Phaser (second generation) diffractometer at room temperature. Samples were irradiated by Co Kα radiation (λ = 1.790 Å) at 30 kV and 10 mA. Used catalysts were slowly passivated in static air at room temperature prior to analysis.

Rietveld refinement was performed using Bruker DIFFRAC. SUITE TOPAS software by fitting CuO (monoclinic, *C2/c*) and ZnO (hexagonal, $P6_3mc$) crystallographic data as Lorentzian functions between *ca.* 36° and 48° 2θ. No crystal strain or preferred orientation in the lattice planes were incorporated. The background was fitted as a first order Chebyshev polynomial, thereby taking the complete diffractogram into account. The y-coordinate of the O atom in CuO and the z-coordinate of the O atom in ZnO were refined. Crystallite sizes were obtained after the fitting converged to a minimum goodness-of-fit (GOF) value.

2.3.4. H_2-TPR profiling

Temperature-programmed reduction (TPR) by H_2 was performed on a Micromeritics AutoChem II 2920 apparatus. Prior to the reduction the sample (50 mg, <75 μm granulites) was dried at 393 K under an Ar flow of 50 mL min^{-1} for 30 min and cooled down to room temperature. Reduction profiles were recorded with a thermal conductivity detector (TCD) when the samples were exposed to a 5% H_2/Ar flow of 50 mL min^{-1} up to 873 K with a ramp of 2 K min^{-1}. H_2O was captured with a dry ice/isopropanol cold trap.

2.4. Catalytic performance measurements

Catalysts were evaluated in a 16-reactor setup (Flowrence, Avantium) for 160 h, operating at 40 bar(g) and 533 K using a H_2/($CO + CO_2$) molar ratio of 2. The catalysts powders were pelletized under a maximum pressure of 1 ton and sieved in granulites between 75 and 150 μm. The stainless steel reactors (inner diameter of 2.6 mm) were loaded with 178 mg 10-Cu/C, 51 mg 6-$CuZnO_x$/C or 6 mg commercial Cu/ZnO/Al_2O_3/MgO catalysts and diluted with inert SiC (sieve fraction of 212–425 μm). This resulted in an inert fraction by SiC between 25 and 92 vol%, thereby minimizing the error by dilution to a maximum of *ca.* 3% [52]. The different sizes of the sieve fractions between the catalysts and diluent facilitated post-analysis by EM and X-ray diffraction (XRD).

First, an *in situ* reduction was performed in 2.8 mL min^{-1} of 5% H_2/N_2 at 523 K for 3 h. The temperature was lowered to 393 K before the reactors were flushed with syngas (H_2/CO/He = 60/30/10 vol%) at a GHSV of 400, 1,400 or 24600 h^{-1} for 1 h for the 10-Cu/C, 6-$CuZnO_x$/C and commercial catalysts, respectively. A tri-phase carbonyl trap (active carbon, γ-Al_2O_3, ZnO) was located upstream the CO feed to remove metal carbonyls and sulfur species. The flows and catalyst loadings were adjusted to compensate for differences in Cu loading (8 *vs* 58 wt%) and packing densities of the sieved catalysts (0.52 *vs* 1.09 g mL^{-1}) to achieve conversions in the same range.

Next, the reactors were pressurized to 40 bar(g) and heated to the reaction temperature of 533 K with a ramp of 2 K min^{-1}. After obtaining catalytic data for 40 h in a H_2/CO/He gas atmosphere a small amount of CO was replaced by CO_2 and the gas composition was equilibrated for 1 h. After 30 h on stream in a CO_2-enriched feed, the CO_2 content was stepwise further increased in a similar way up to H_2/CO/CO_2/He = 60/23/7/10 vol%. Products were periodically analyzed by online gas chromatography every 15 min. After catalysis the samples were slowly exposed to air at 393 K. The calculations of activity, selectivity and stability are detailed in Section S5.

3. Results and discussion

3.1. Structural properties of the catalysts

First we discuss the particle size and elemental distribution in the catalysts as studied by electron microscopy and energy-dispersive X-ray (EDX) spectroscopy (Table 1). Fig. 1 shows electron micrographs of two selected carbon-supported CuO catalysts, either promoted with ZnO_x or not [53]. In bright-field transmission electron microscopy (BF-TEM) (frames C and A) particles of respectively *ca.* 5.5 nm and 9.3 nm (dark dots) are uniformly distributed over the support surface (light grey). Similarly sized and well-distributed nanoparticles were consistently found throughout these catalysts (more examples in Fig. S1). Elemental mapping (frame E) shows that the ZnO_x in the as-synthesized 6-$CuZnO_x$/C catalyst was evenly dispersed over the support surface and that the observed particles in BF-TEM (frames A and C) were hence mostly consisting of Cu(O). However, the elemental distribution after high-pressure methanol synthesis (frame F) is probably more representative of the catalyst during action, and demonstrates a close intimacy between the Cu and Zn species. The high surface area carbon support consisted of stacked graphitic sheets and exhibited a surface area of 509 m^2 g^{-1} and a mesopore volume of 0.36 mL g^{-1}, while after Cu and Zn deposition 297 m^2 g^{-1} and 0.23 mL g^{-1} were obtained (Section S2). The high surface area of the carbon support clearly allowed a uniform distribution of nanoparticles over the support [46,54–56].

Frames B and D show that the CuO particle sizes were distributed in a lognormal fashion for the fresh 10-Cu/C and 6-$CuZnO_x$/C catalysts. Based on the histograms the particle size distribution was also translated into a surface-averaged size, which is relevant for catalysis, and a volume-averaged size, which can be directly compared to X-ray diffraction (XRD) [57,58] (Table 1). A few agglomerates were present in the used catalysts (Fig. S7) but not taken into account in the corresponding particle size averages obtained from BF-TEM. The preparation and characterization of 10-$CuZnO_x$/C catalysts containing 0.1 wt% ZnO was reproduced three times (Fig. S2). For all three 10-$CuZnO_x$/C catalysts similar number-averaged particle sizes (7.6 ± 1.1 nm) and distributions were obtained, proofing that the catalyst synthesis was reproducible. All three carbon-supported catalysts shown in Table 1 had a similar Cu loading (8.1 ± 0.3 wt%), which was confirmed by temperature-programmed reduction with H_2 (7.7 ± 1.4 wt%, Fig. S3). These results show that the presence of sufficient ZnO_x, as in the 6-$CuZnO_x$/C catalyst, limited the growth of CuO_x nanoparticles during catalyst synthesis.

Powder X-ray diffraction patterns of the as-synthesized 10-Cu/C and 6-$CuZnO_x$/C catalysts (Fig. 2, frame A) showed, next to the graphite diffraction lines at 30.7° and 50.4° 2θ, only diffractions attributed to CuO crystallites at 37.9°, 41.4°, 45.2° and 57.1° 2θ. The crystallite sizes were respectively *ca.* 16 and 6 nm and corresponded to the volume-averaged CuO particle sizes, derived from the BF-TEM particle size histograms, of 10.4 ± 3.5 nm and 6.2 ± 2.0 nm, respectively. No diffraction peaks due to ZnO were observed for the fresh 6-$CuZnO_x$/C catalyst, which is in line with the high ZnO_x dispersion observed in the fresh catalyst with elemental mapping (Fig. 1, frame E). After catalysis the ZnO (partly) crystallized (Fig. 2, frame B), showing crystallites of 12 nm. This observation was in agreement with the fact that in the used 6-$CuZnO_x$/C catalyst also some larger particles were found in the sample (Fig. S7). In both used 10-Cu/C and 6-$CuZnO_x$/C catalysts (frame B) the diffractions at 50.6° and 59.1° 2θ are attributed to 13 and 12 nm Cu^0 crystallites, respectively. Please note that these Cu^0 sizes are slightly smaller than the CuO sizes in the fresh catalysts (Table 1), but this difference may be explained by the fact that not all Cu is in the metallic phase. Due to passivation of the samples after catalysis different phases of copper oxide were present.

As a reference also a commercial Cu/ZnO/Al_2O_3/MgO methanol synthesis catalyst (com cat) prepared by co-precipitation [5,10,34,35,44,59] was included (Table 1, Fig. 2, Figs. S4–S5). XRD analysis in Fig. 2 (frame A) shows diffractions at 35°, 38° and 42° 2θ attributed to ZnO and with a width corresponding to an approximate crystallite size of 4 nm. The catalyst typically contained *ca.* 10 nm-sized Cu(O) particles [10] and 58 wt% Cu with a Zn/(Cu + Zn) molar fraction of 0.28, which was similar to our 10-$CuZnO_x$/C catalyst (0.35). The commercial catalyst is known to have a close intimacy of Cu and Zn species (Fig. S4), whereas Al_2O_3 mainly acts as a spacer [7–9].

3.2. Influence of ZnO_x on activity and selectivity during CO hydrogenation

First we tested methanol synthesis with only CO and H_2 in the feed (hence, without CO_2). Fig. 3 (frame A) shows the CO conver-

Table 1
Overview of structural properties of selected catalysts.

Catalyst	Loading (wt%)		TEM CuO particle size[A] (nm)		XRD CuO crystallite size[B] (nm)
	Cu	ZnO	d_S	d_V	
10-Cu/C (fresh)	8.1	0	9.9 ± 3.3	10.4 ± 3.5	15.9 ± 0.5
10-Cu/C (used)			12.6 ± 5.8	14.4 ± 6.5	13[C]
10-$CuZnO_x$/C	8.4	0.1	9.6 ± 4.3	10.7 ± 4.7	–
6-$CuZnO_x$/C (fresh)	7.7	5.3	5.8 ± 1.9	6.2 ± 2.0	5.8 ± 0.5
6-$CuZnO_x$/C (used)			8.8 ± 3.1	9.4 ± 3.3	12[C]
Cu/ZnO/Al_2O_3/MgO (com cat) (fresh)	58.4	28.4	*ca.* 10		5.8 ± 0.1

[A] Average CuO sizes with width of the particle size distribution.
[B] Error indicates fitting error by Rietveld refinement of CuO.
[C] Cu^0 crystallite size estimated from Scherrer equation at 59° 2θ, excluding CuO_x.

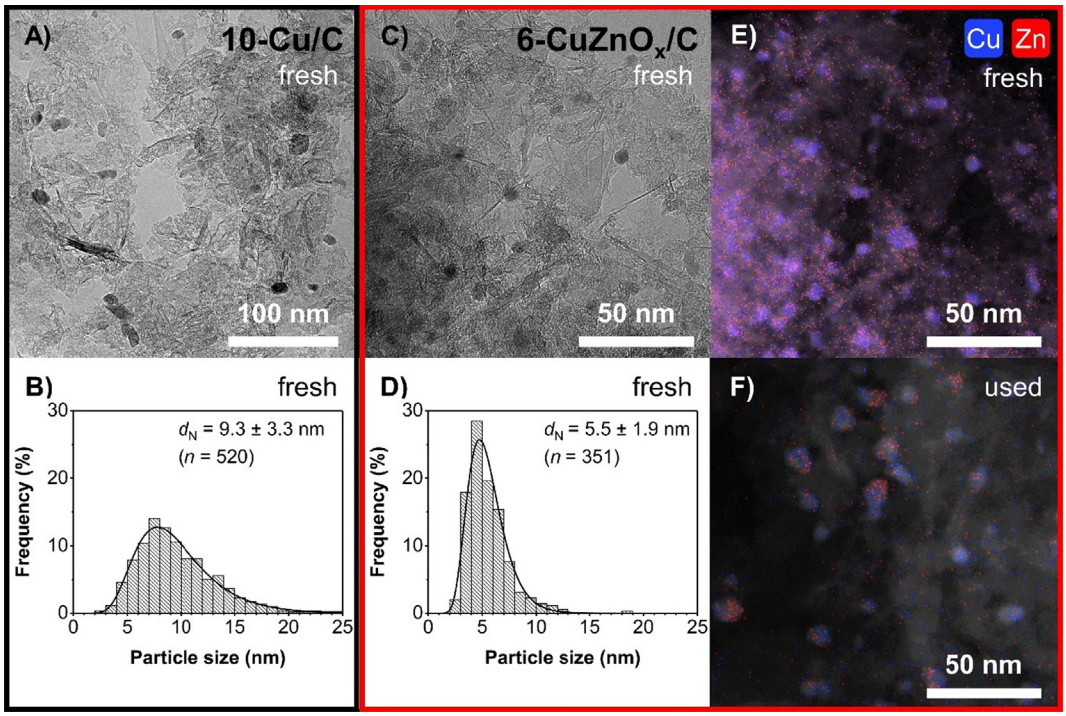

Fig. 1. (A, C) Representative BF-TEM images and (B, D) corresponding particle size distributions of (A, B) the fresh 10-Cu/C catalyst (8.1 wt%) and (C, D) the fresh 6-$CuZnO_x$/C catalyst (7.7 wt% Cu, 5.3 wt% ZnO). Surface-averaged CuO particle sizes were 9.9 ± 3.3 nm and 5.8 ± 1.9 nm, respectively. Elemental distribution of Cu and Zn in (E) the fresh 6-$CuZnO_x$/C catalyst in the same area of frame C and (F) the used 6-$CuZnO_x$/C catalyst.

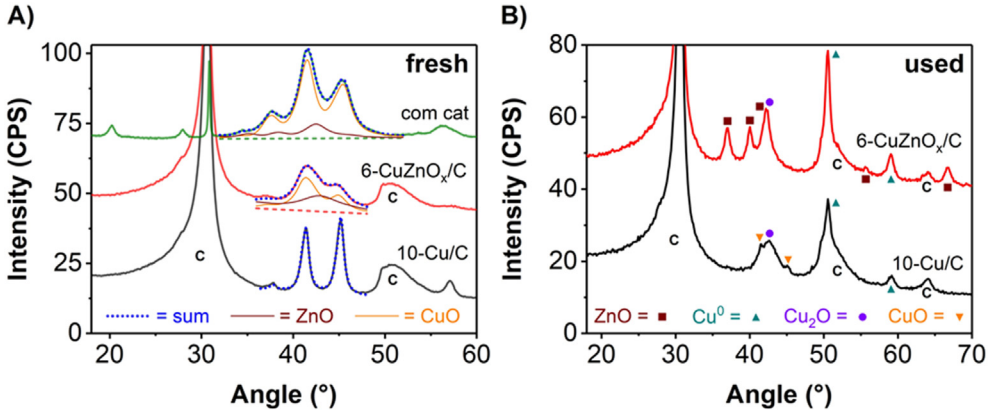

Fig. 2. Powder X-ray diffractograms of (A) selected fresh catalysts and (B) used catalysts after 160 h of catalysis and subsequent passivation. The diffractograms are vertically offset for clarity. The blue dotted lines represent Rietveld fittings and the dashed lines describe the corresponding backgrounds. The peaks below 35° 2θ in the com cat were due to mixed metal oxides, based on Al and/or Mg.

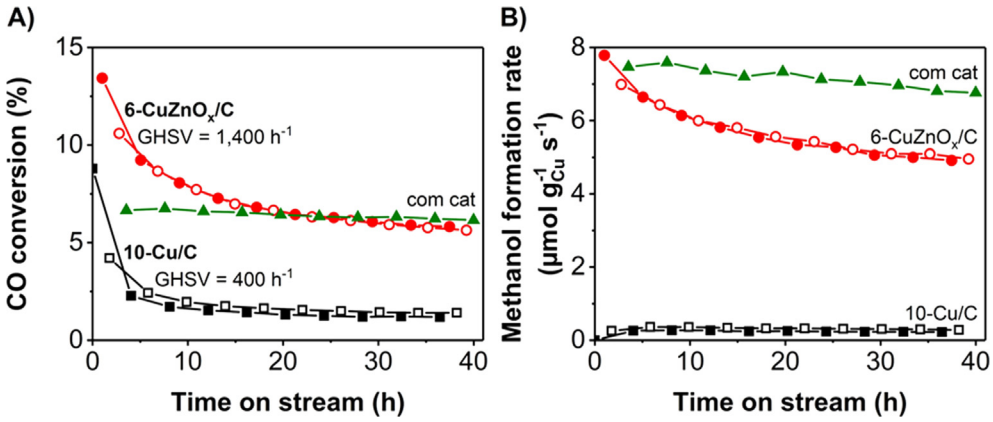

Fig. 3. (A) CO conversion and (B) methanol formation rate over time during CO hydrogenation. Hollow symbols represent a duplicate test from the same catalyst batch. Conditions: 533 K, 40 bar(g), H_2/CO/He = 60/30/10 vol%, flow = 152, 560, 620 mL min^{-1} g_{Cu}^{-1} and GHSV = 400, 1,400, 24,600 h^{-1} for 10-Cu/C, 6-CuZnO$_x$/C and com cat, respectively.

sion as a function of time for two selected catalysts, 10-Cu/C and 6-CuZnO$_x$/C, as well as for the commercial Cu/ZnO/Al_2O_3/MgO catalyst to put our catalysts into perspective. The commercial catalyst was stable from the start, probably because it had already been exposed to temperatures >573 K [10,44], although the stabilizing effect by Al and/or Mg species could also play a role [5]. For both carbon-supported catalysts an activation period of *ca.* 20 h was observed, which can be explained by the fact that this was the first time that they were subjected to 533 K and high pressure. The hollow symbols represent a duplicate test from the same catalyst batch, proving that the catalytic testing was reproducible. All these conversion levels are well below the thermodynamic equilibrium of 35.7% (see Table S3 for further details) [60,61].

Table 2 shows the CO conversion, also normalized to the Cu mass in the reactor, as well as the turnover frequencies based on the particle sizes in the fresh and used catalysts. Note that these different activities are not directly reflected in Fig. 3 (frame A) as for these tests the flows and catalyst loadings were adjusted to compensate for differences in Cu loading and packing densities, in order to achieve conversion levels in the same range. By comparing the activities of the 10-Cu/C and 6-CuZnO$_x$/C catalysts it is clear that the ZnO$_x$ addition led to an activity increase of about one order of magnitude. After 40 h on stream our 6-CuZnO$_x$/C catalyst had a methanol turnover frequency of $2.7{\cdot}10^{-3}$ s^{-1}, which was similar to the commercial Cu/ZnO/Al_2O_3/MgO catalyst with an activity of *ca.* $2.4{\cdot}10^{-3}$ s^{-1}. The turnover frequency of the 6-CuZnO$_x$/C catalyst may be even higher as a few agglomerates were found in this catalyst, but not taken into account in the particle size average (Fig. S7). As mentioned earlier in the introduction, only a few and somewhat contradictory studies are available regarding the effect of ZnO$_x$ while hydrogenating pure CO, which might be induced by the use of (different) oxidic supports. Therefore, we studied the effect of ZnO$_x$ addition during CO hydrogenation while using an inert graphitic support [42].

Fig. 3 (frame B) presents the evolution of the methanol formation rate over time. After the activation period all catalysts showed a stable methanol production. However, the methanol formation rate (and selectivity from Table 2) was surprisingly low (<8 μmol g_{Cu}^{-1} s^{-1}), even for the commercial catalyst, compared to what is typically reported for CO_2-enriched syngas conversion [44,47]. This might be induced by a slight deficiency in hydrogen [61] and the slightly high reaction temperature. Although there are few old studies available on Cu/ZnO/Al_2O_3 catalysts [21,23,24], as far as we are aware this is the first time that the methanol formation rates are reported for carbon-supported Cu particles in the presence and absence of ZnO$_x$ during pure CO hydrogenation.

Fig. 4 displays the evolution of the other products formed over the 10-Cu/C and 6-CuZnO$_x$/C catalysts, averaged over at least four separate measurement runs. In both cases CO_2 was the main side product, but also hydrocarbons, ethanol and, in the case of the 6-CuZnO$_x$/C catalyst, dimethyl ether (DME) were detected. The hydrocarbon formation rates were *ca.* 4 orders of magnitude lower than typically found in iron-based Fischer-Tropsch synthesis [62]. DME was probably formed by dehydration of methanol ($2CH_3OH \rightarrow (CH_3)_2O + H_2O$) [63] on the acidic oxygen vacancy sites on the ZnO$_x$ surface [64,65]. Interestingly, CO_2 was produced from CO, while no water or oxygen was present in the feed. Other oxygen sources such as ZnO$_x$ or contaminations in the feed, SiC diluent and/or carbonyl trap were excluded (Section S4). This CO_2 production could be explained by the co-formation of hydrocarbons, ethanol and DME. The total formation rate of these compounds for the 10-Cu/C catalyst ($5.1 \pm 1.1{\cdot}10^{-8}$ mol g_{Cu}^{-1} s^{-1}) was similar to the rate

Table 2
Overview of catalytic results during CO hydrogenation in the absence of CO_2. The initial turnover frequency (TOF) was calculated using the CuO particle size in the fresh catalyst and the activity at t = 0. The final TOF was estimated from the CuO particle size after 160 h of catalysis (see also Fig. S6) and the activity at t = 40 h. The methanol selectivity included CO_2 in the product distribution. The errors indicate the standard deviation between two measurements unless stated otherwise. Conditions were equal to Fig. 3.

Catalyst	GHSV (h^{-1})	CO conversion (%)		CO conversion rate (μmol g_{Cu}^{-1} s^{-1})		Total turnover frequency[A] (10^{-3} s^{-1})		MeOH selectivity (%$_C$)	
		0 h	40 h	0 h	40 h	0 h	40 h	0 h	40 h
10-Cu/C	400	8.8	1.3 ± 0.1	2.1	0.4	1.6 ± 0.6	0.3 ± 0.1	0	63 ± 5
6-CuZnO$_x$/C	1,400	15.1	5.7 ± 0.1	21.5	6.5	6.1 ± 2.0	3.5 ± 1.2	48	75 ± 1
com cat	24,600	6.8	6.2	8.7	7.7	3.0[B]	2.7[B]	89	88

[A] The error in the TOF reflects the width in the CuO particle size distribution from BF-TEM.
[B] The CuO crystallite size (from XRD) in the fresh catalyst was used in the calculation.

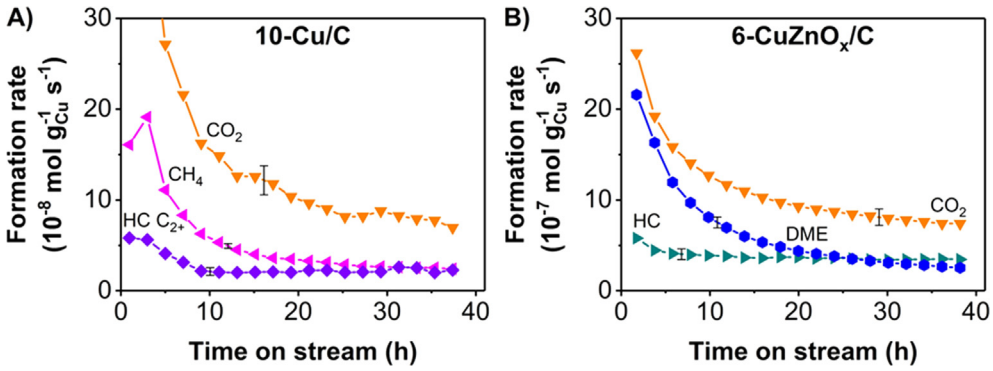

Fig. 4. Time evolution of side product formation rates during CO hydrogenation for the (A) 10-Cu/C and (B) 6-$CuZnO_x$/C catalysts. Mind the order of magnitude difference between the frames. All points are the average over four or six separate measurement runs, with the error bars indicating the spread. Less than $0.4 \pm 0.5 \cdot 10^{-8}$ and $0.4 \pm 0.2 \cdot 10^{-7}$ mol g_{Cu}^{-1} s^{-1} ethanol was formed, respectively. HC = hydrocarbons, DME = dimethyl ether. Conditions were equal to Fig. 3.

of produced CO_2 after 40 h of catalysis ($6.9 \pm 3.1 \cdot 10^{-8}$ mol g_{Cu}^{-1} s^{-1}). An analogous observation was made for the 6-$CuZnO_x$/C catalyst ($6.3 \pm 1.7 \cdot 10^{-7}$ *vs* $7.2 \pm 1.8 \cdot 10^{-7}$ mol g_{Cu}^{-1} s^{-1}). Hence, the following reaction plausibly occurred (next to direct CO hydrogenation to methanol [10,21,23–27,63]): $2xCO + (x + 1)H_2 \rightarrow xCO_2 + C_xH_{2x+2}$.

An intriguing question is why the produced CO_2 was not (entirely) consumed by hydrogenation to methanol. From literature it is known that CO_2 is preferred over CO as the carbon source for methanol production at high temperatures [11,28]. The CO_2 concentration in these systems is very low with a corresponding partial pressure of 0.04 and 0.11 bar for, respectively, the 10-Cu/C and 6-$CuZnO_x$/C catalysts after 40 h on stream, as CO_2 was only generated during the reaction. To our knowledge this is the first time that these relatively low methanol selectivities in a pure H_2/CO feed have been reported and tentatively explained.

3.3. Combined influence of CO_2 and ZnO_x

In industrial methanol production a CO_2-enriched syngas feed is typically used [20]. Fig. 5 (frame A) shows the effect of CO_2 concentration in the syngas feed on the CO + CO_2 conversion for carbon-supported Cu catalysts with and without ZnO_x as well as for the commercial catalyst. Please note that this is the net conversion, as we cannot determine the extent of (reverse) WGS taking place in the reactor. The conversion is taken after at least 30 h on stream in a specific gas composition (for the time evolution see Fig. S6). Even 1 vol% CO_2 in the feed (obtained by replacing 3% of the CO with CO_2) increased the CO + CO_2 conversion for the 6-$CuZnO_x$/C catalyst from 5.7% to 11.9% and with 3 vol% CO_2 in the feed the maximum CO + CO_2 conversion was reached, while with even higher CO_2 content the conversion level again decreased, down to 6.8% with 7 vol% CO_2 in the total feed. An effect of CO_2 in syngas on the conversion has been observed earlier [6,11,20–23,38,39]. A similar conversion increase was observed for the commercial catalyst for low and increasing CO_2 concentrations, but the decline at higher concentrations was much less pronounced.

The decrease in the conversion level for the 6-$CuZnO_x$/C catalyst at higher CO_2 concentrations in the feed (frame A) could be explained by a combination of Cu particle growth, ZnO_x promotion loss and/or Cu surface oxidation. TEM analysis (Table 1) showed only a minor CuO_x particle growth to 8.8 ± 3.1 nm in the used 6-$CuZnO_x$/C catalyst, although probably a significant amount of the Cu atoms were located in several larger particles, but contributing little to the active surface area (Fig. S7). XRD analysis of the used catalyst (Fig. 2, frame B) indicated a significant ZnO crystallization to approximately 12 nm, even though a close interaction between ZnO_x and Cu was preserved (Fig. 1, frame F, Fig. S7). Another possible consequence of the higher CO_2 concentration (and the additional H_2O formation), and hence a more oxidizing atmosphere, could be a higher oxygen coverage of the Cu surface, which is reported to render the catalyst less active [6,22,27].

The influence of CO_2 in the syngas feed on the activity of unpromoted supported Cu particles was so far not clear, as reported results varied depending on the type of oxidic support used [25,27]. Furthermore, as we also found (Fig. S8), Cu-based catalysts can show a relatively long activation period and performance might be influenced on the activation protocol, which is a topic of further study. However, based on carbon-supported model catalysts we clearly show that for unpromoted Cu nanoparticles, in the absence of any oxidic phase, the syngas conversion level (Fig. 5, frame A) is not significantly influenced by the CO_2 content. Hence, synergy between Cu nanoparticles and ZnO_x (or another appropriate oxidic promoter) is clearly needed for effective CO_2 hydrogenation, which plays such an important role in the industrial methanol synthesis process [27,66].

Fig. 5 (frame B) presents the methanol selectivity of the catalysts in different syngas compositions, thereby not taking CO_2 in account as a possible product in the product distribution, as a function of the CO_2 content in the feed (for the time evolution see Fig. S6). Interestingly, a modest addition of CO_2 boosted the methanol selectivity by *ca.* $8\%_C$ for the 6-$CuZnO_x$/C and 10-Cu/C catalysts. In CO_2-enriched syngas feeds the commercial catalyst reached a methanol selectivity of $>99\%_C$, which was also reported by our group at similar CO + CO_2 conversion levels [47,67]. The lower selectivity for the 10-Cu/C catalyst ($89\%_C$) was also observed for a Cu/SiO_2 catalyst ($92\%_C$) and might be caused by its low conversion level [68]. It has to be noted that the hydrocarbon formation rate was similar in all syngas atmospheres ($2.7 \cdot 10^{-7}$ mol g_{Cu}^{-1} s^{-1} or $1.5 \cdot 10^{-4}$ s^{-1} for the 6-$CuZnO_x$/C catalyst), showing that the methanol selectivity increase was governed by an increased methanol formation rate (see also Table S2). This remarkable improvement with the addition of a small amount of CO_2 can be understood for the 6-$CuZnO_x$/C catalyst by the DME suppression, as sufficient H_2O was generated *via* the CO_2 hydrogenation to methanol. Additionally, the higher H_2O content seems to play a role in lowering of the C—O bond dissociation activity with respect to the methanol formation rate, as discussed in detail in Section 3.2.

Fig. 5 (frame C) illustrates the methanol turnover frequency (TOF_{MeOH}), serving as a combination of the CO + CO_2 conversion (frame A) and the CO_2-free methanol selectivity (frame B). For the ZnO_x-promoted catalysts, the trends in the TOF_{MeOH} reflect those of the CO + CO_2 conversion. Also, our 6-$CuZnO_x$/C catalyst performed in the same order of magnitude as the commercial catalyst, hence illustrating the relevance of our model catalyst study.

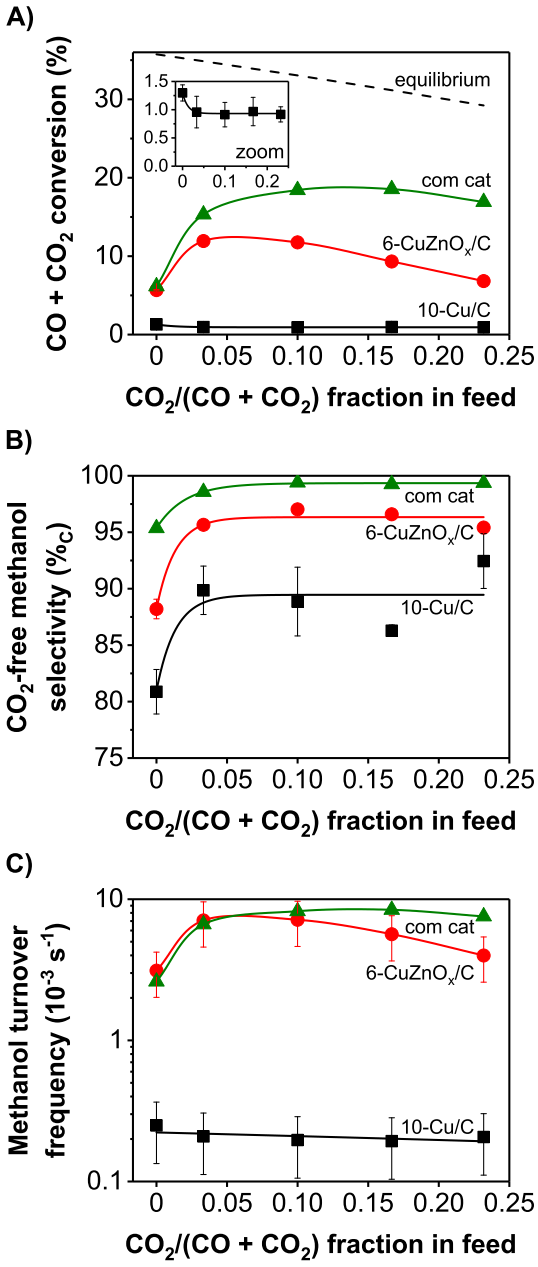

Fig. 5. (A) Net CO + CO_2 conversion, (B) carbon atom-based methanol selectivity, thereby not taking CO_2 in account as a possible product in the product distribution (see also Equation (S11)), and (C) methanol turnover frequency (TOF_{MeOH}) at different syngas compositions. The catalysts were exposed to increasing CO_2 concentrations in the feed at a constant H_2/(CO + CO_2) ratio. Values were determined after 30 h on stream in a specific gas composition (40 h on stream for no CO_2 in feed). The TOF_{MeOH} was estimated using the CuO particle size after 160 h of catalysis. Error bars represent the standard deviations between two measurements (frames A and B) or reflect the width in the CuO size distribution in the used catalysts (frame C). Conditions: H_2/CO + CO_2/He = 60/30/10 vol%, further equal to Fig. 3.

The slightly lower conversion at higher CO_2 contents in the feed might be explained by an increased loss of ZnO_x promoter effect by crystallization, dealloying and/or overcoverage over active Cu surface area [30,39] compared to the stabilized commercial catalyst by metal oxides. For the 10-Cu/C catalyst the TOF_{MeOH} (frame C) did not change at all ($2.1 \cdot 10^{-4}$ s^{-1}) upon CO_2 enrichment of the feed, again strongly suggesting that the Cu catalyst alone is quite inactive in CO_2 hydrogenation.

4. Conclusions

We prepared a series of carbon-supported $CuZnO_x$ catalysts with a uniform distribution of Cu nanoparticles and, when present, ZnO_x in close contact with Cu during catalysis. While hydrogenating pure CO ZnO_x promoted the activity by about one order of magnitude and led next to methanol to the production of dimethyl ether. A maximum activity of the promoted catalyst was obtained with 3 vol% CO_2 enrichment of the syngas, whereas the methanol formation rate over unpromoted Cu was not influenced by CO_2 addition. Interestingly, alternative products (>10%$_C$) such as CO_2 and hydrocarbons were formed for all catalysts in the absence of CO_2 in the feed in concomitance with methanol. The methanol selectivity of all catalysts was very high when CO_2 was present in the feed.

Declaration of Competing Interest

The authors declare that they have no known competing financial interests or personal relationships that could have appeared to influence the work reported in this paper.

Acknowledgments

Rolf Beerthuis and Jan Willem de Rijk are thanked for input during catalytic testing. This project has received funding from the European Research Council (ERC), ERC-2014-CoG, project number 648991.

Appendix A. Supplementary data

Supplementary data to this article can be found online at https://doi.org/10.1016/j.jcat.2020.10.006.

References

[1] J. Sehested, Industrial and scientific directions of methanol catalyst development, J. Catal. 371 (2019) 368–375, https://doi.org/10.1016/j.jcat.2019.02.002.
[2] G.A. Olah, Beyond oil and gas: The methanol economy, Angew. Chem. Int. Ed. 44 (18) (2005) 2636–2639, https://doi.org/10.1002/anie.200462121.
[3] Methanol Institute, Methanol price and supply/demand, 2020. https://www.methanol.org/methanol-price-supply-demand/ (accessed June 15, 2020).
[4] M. Alvarado, The changing face of the global methanol market, IHS, Chem. Bull. (2016) 1–2.
[5] Almusaiteer K.A., Al-Hadhrami A., Abed O., Biausque G., Al-Amer A., Catalysts and methods for methanol synthesis from direct hydrogenation of syngas and/or carbon dioxide, US20190076828A1 (2019).
[6] K.C. Waugh, Methanol synthesis, Catal. Today 15 (1) (1992) 51–75, https://doi.org/10.1016/0920-5861(92)80122-4.
[7] F. Zhang, Y. Liu, X. Xu, P. Yang, P. Miao, Y. Zhang, Q. Sun, Effect of Al-containing precursors on Cu/ZnO/Al_2O_3 catalyst for methanol production, Fuel Process. Technol. 178 (2018) 148–155, https://doi.org/10.1016/j.fuproc.2018.04.021.
[8] G. Prieto, K.P. de Jong, P.E. de Jongh, Towards 'greener' catalyst manufacture: Reduction of wastewater from the preparation of Cu/ZnO/Al_2O_3 methanol synthesis catalysts, Catal. Today 215 (2013) 142–151, https://doi.org/10.1016/j.cattod.2013.03.033.
[9] R. Guil-López, N. Mota, J. Llorente, E. Millán, B. Pawelec, R. García, J.L.G. Fierro, R.M. Navarro, Structure and activity of Cu/ZnO catalysts co-modified with aluminium and gallium for methanol synthesis, Catal. Today (2019), https://doi.org/10.1016/j.cattod.2019.03.034.
[10] M. Behrens, F. Studt, I. Kasatkin, S. Kühl, M. Hävecker, F. Abild-Pedersen, S. Zander, F. Girgsdies, P. Kurr, B.-L. Kniep, M. Tovar, R.W. Fischer, J.K. Nørskov, R. Schlögl, The active site of methanol synthesis over Cu/ZnO/Al_2O_3 industrial catalysts, Science 336 (6083) (2012) 893–897, https://doi.org/10.1126/science.1219831.
[11] I. Abbas, H. Kim, C.-H. Shin, S. Yoon, K.-D. Jung, Differences in bifunctionality of ZnO and ZrO_2 in Cu/ZnO/ZrO_2/Al_2O_3 catalysts in hydrogenation of carbon oxides for methanol synthesis, Appl. Catal. B 258 (2019) 117971, https://doi.org/10.1016/j.apcatb.2019.117971.
[12] C. Si, H. Ban, K. Chen, X. Wang, R. Cao, Q. Yi, Z. Qin, L. Shi, Z. Li, W. Cai, C. Li, Insight into the positive effect of Cu^0/Cu^+ ratio on the stability of Cu-ZnO-CeO_2 catalyst for syngas hydrogenation, Appl. Catal. A 594 (2020) 117466, https://doi.org/10.1016/j.apcata.2020.117466.

[13] J. Schumann, M. Eichelbaum, T. Lunkenbein, N. Thomas, M.C. Álvarez Galván, R. Schlögl, M. Behrens, Promoting strong metal support interaction: Doping ZnO for enhanced activity of Cu/ZnO:M (M = Al, Ga, Mg) catalysts, ACS Catal. 5 (6) (2015) 3260–3270, https://doi.org/10.1021/acscatal.5b00188.
[14] W.J. Lee, A. Bordoloi, J. Patel, T. Bhatelia, The effect of metal additives in Cu/Zn/Al_2O_3 as a catalyst for low-pressure methanol synthesis in an oil-cooled annulus reactor, Catal. Today 343 (2020) 183–190, https://doi.org/10.1016/j.cattod.2019.03.041.
[15] G. Wang, Y. Zuo, M. Han, J. Wang, Copper crystallite size and methanol synthesis catalytic property of Cu-based catalysts promoted by Al, Zr and Mn, React. Kinet. Mech. Catal. 101 (2) (2010) 443–454, https://doi.org/10.1007/s11144-010-0240-9.
[16] I. Sharafutdinov, C.F. Elkjær, H.W. Pereira de Carvalho, D. Gardini, G.L. Chiarello, C.D. Damsgaard, J.B. Wagner, J.-D. Grunwaldt, S. Dahl, I. Chorkendorff, Intermetallic compounds of Ni and Ga as catalysts for the synthesis of methanol, J. Catal. 320 (2014) 77–88, https://doi.org/10.1016/j.jcat.2014.09.025.
[17] T.E.L. Smitshuysen, M.R. Nielsen, T. Pruessmann, A. Zimina, T.L. Sheppard, J.-D. Grunwaldt, I. Chorkendorff, C.D. Damsgaard, Optimizing Ni–Fe–Ga alloys into Ni_2FeGa for the hydrogenation of CO_2 into methanol, ChemCatChem 12 (12) (2020) 3265–3273, https://doi.org/10.1002/cctc.202000174.
[18] E.M. Fiordaliso, I. Sharafutdinov, H.W.P. Carvalho, J.-D. Grunwaldt, T.W. Hansen, I. Chorkendorff, J.B. Wagner, C.D. Damsgaard, Intermetallic $GaPd_2$ nanoparticles on SiO_2 for low-pressure CO_2 hydrogenation to methanol: catalytic performance and in situ characterization, ACS Catal. 5 (10) (2015) 5827–5836, https://doi.org/10.1021/acscatal.5b01271.
[19] Curulla-Ferré D., Drouilly C., Martin O., Mondelli C., Pérez-Ramírez J., Martin-Fernandez A.J., Supported indium oxide catalyst and process for methanol synthesis using the same, US20200061582A1 (2020).
[20] G. Iaquaniello, B. Cucchiella, E. Antonetti, Method for producing synthesis gas for methanol production, WO2013062413A1, 2013.
[21] K. Klier, V. Chatikavanij, R.G. Herman, G.W. Simmons, Catalytic synthesis of methanol from CO/H_2: IV. The effects of carbon dioxide, J. Catal. 74 (1982) 343–360, https://doi.org/10.1016/0021-9517(82)90040-9.
[22] M. Sahibzada, I.S. Metcalfe, D. Chadwick, Methanol synthesis from $CO/CO_2/H_2$ over $Cu/ZnO/Al_2O_3$ at differential and finite conversions, J. Catal. 174 (2) (1998) 111–118, https://doi.org/10.1006/jcat.1998.1964.
[23] J.S. Lee, K.H. Lee, S.Y. Lee, Y.G. Kim, A comparative study of methanol synthesis from CO_2/H_2 and CO/H_2 over a $Cu/ZnO/Al_2O_3$ catalyst, J. Catal. 144 (2) (1993) 414–424, https://doi.org/10.1006/jcat.1993.1342.
[24] R.M. Agny, C.G. Takoudis, Synthesis of methanol from carbon monoxide and hydrogen over a copper-zinc oxide-alumina catalyst, Ind. Eng. Chem. Prod. Res. Dev. 24 (1) (1985) 50–55, https://doi.org/10.1021/i300017a010.
[25] N.D. Nielsen, J. Thrane, A.D. Jensen, J.M. Christensen, Bifunctional synergy in CO hydrogenation to methanol with supported Cu, Catal. Lett. 150 (5) (2020) 1427–1433, https://doi.org/10.1007/s10562-019-03036-7.
[26] Z.-J. Zuo, P.-D. Han, Z. Li, J.-S. Hu, W. Huang, Can methanol be synthesized from CO by direct hydrogenation over Cu/ZnO catalysts?, Appl. Surf. Sci. 261 (2012) 640–646, https://doi.org/10.1016/j.apsusc.2012.08.074.
[27] F. Studt, M. Behrens, E.L. Kunkes, N. Thomas, S. Zander, A. Tarasov, J. Schumann, E. Frei, J.B. Varley, F. Abild-Pedersen, J.K. Nørskov, R. Schlögl, The mechanism of CO and CO_2 hydrogenation to methanol over Cu-based catalysts, ChemCatChem 7 (2015) 1105–1111, https://doi.org/10.1002/cctc.201500123.
[28] Y. Yang, C.A. Mims, D.H. Mei, C.H.F. Peden, C.T. Campbell, Mechanistic studies of methanol synthesis over Cu from $CO/CO_2/H_2/H_2O$ mixtures: The source of C in methanol and the role of water, J. Catal. 298 (2013) 10–17, https://doi.org/10.1016/j.jcat.2012.10.028.
[29] O. Martin, J. Pérez-Ramírez, New and revisited insights into the promotion of methanol synthesis catalysts by CO_2, Catal. Sci. Technol. 3 (12) (2013) 3343–3352, https://doi.org/10.1039/c3cy00573a.
[30] J. Wu, M. Saito, M. Takeuchi, T. Watanabe, The stability of Cu/ZnO-based catalysts in methanol synthesis from a CO_2-rich feed and from a CO-rich feed, Appl. Catal. A 218 (1-2) (2001) 235–240, https://doi.org/10.1016/S0926-860X(01)00650-0.
[31] G. Prieto, J.D. Meeldijk, K.P. de Jong, P.E. de Jongh, Interplay between pore size and nanoparticle spatial distribution: Consequences for the stability of CuZn/SiO_2 methanol synthesis catalysts, J. Catal. 303 (2013) 31–40, https://doi.org/10.1016/j.jcat.2013.02.023.
[32] R. van den Berg, T.E. Parmentier, C.F. Elkjær, C.J. Gommes, J. Sehested, S. Helveg, P.E. de Jongh, K.P. de Jong, Support functionalization to retard Ostwald ripening in copper methanol synthesis catalysts, ACS Catal. 5 (7) (2015) 4439–4448, https://doi.org/10.1021/acscatal.5b00833.
[33] R. van den Berg, J. Zečević, J. Sehested, S. Helveg, P.E. de Jongh, K.P. de Jong, Impact of the synthesis route of supported copper catalysts on the performance in the methanol synthesis reaction, Catal. Today 272 (2016) 87–93, https://doi.org/10.1016/j.cattod.2015.08.052.
[34] M.B. Fichtl, D. Schlereth, N. Jacobsen, I. Kasatkin, J. Schumann, M. Behrens, R. Schlögl, O. Hinrichsen, Kinetics of deactivation on $Cu/ZnO/Al_2O_3$ methanol synthesis catalysts, Appl. Catal. A 502 (2015) 262–270, https://doi.org/10.1016/j.apcata.2015.06.014.
[35] T. Lunkenbein, F. Girgsdies, T. Kandemir, N. Thomas, M. Behrens, R. Schlögl, E. Frei, Bridging the time gap: A copper/zinc oxide/aluminum oxide catalyst for methanol synthesis studied under industrially relevant conditions and time scales, Angew. Chem. Int. Ed. 55 (41) (2016) 12708–12712, https://doi.org/10.1002/anie.201603368.
[36] K. Chen, J. Yu, B. Liu, C. Si, H. Ban, W. Cai, C. Li, Z. Li, K. Fujimoto, Simple strategy synthesizing stable $CuZnO/SiO_2$ methanol synthesis catalyst, J. Catal. 372 (2019) 163–173, https://doi.org/10.1016/j.jcat.2019.02.035.
[37] D.B. Rasmussen, T.V.W. Janssens, B. Temel, T. Bligaard, B. Hinnemann, S. Helveg, J. Sehested, The energies of formation and mobilities of Cu surface species on Cu and ZnO in methanol and water gas shift atmospheres studied by DFT, J. Catal. 293 (2012) 205–214, https://doi.org/10.1016/j.jcat.2012.07.001.
[38] Y. Choi, K. Futagami, T. Fujitani, J. Nakamura, The difference in the active sites for CO_2 and CO hydrogenations on Cu/ZnO-based methanol synthesis catalysts, Catal. Lett. 73 (2001) 27–31, https://doi.org/10.1023/A:1009074219286.
[39] S. Kuld, M. Thorhauge, H. Falsig, C.F. Elkjær, S. Helveg, I. Chorkendorff, J. Sehested, Quantifying the promotion of Cu catalysts by ZnO for methanol synthesis, Science 352 (6288) (2016) 969–974, https://doi.org/10.1126/science.aaf0718.
[40] S. Zander, E.L. Kunkes, M.E. Schuster, J. Schumann, G. Weinberg, D. Teschner, N. Jacobsen, R. Schlögl, M. Behrens, The role of the oxide component in the development of copper composite catalysts for methanol synthesis, Angew. Chem. Int. Ed. 52 (25) (2013) 6536–6540, https://doi.org/10.1002/anie.201301419.
[41] Y. Sun, L. Chen, Y. Bao, Y. Zhang, J. Wang, M. Fu, J. Wu, D. Ye, The applications of morphology controlled ZnO in catalysis, Catalysts 6 (2016) 1–44, https://doi.org/10.3390/catal6120188.
[42] R. Chatterjee, S. Kuld, R. van den Berg, A. Chen, W. Shen, J.M. Christensen, A.D. Jensen, J. Sehested, Mapping support interaction in copper catalysts, Top. Catal. 62 (2019) 649–659, https://doi.org/10.1007/s11244-019-01150-9.
[43] M. Che, C.O. Bennett, The influence of particle size on the catalytic properties of supported metals, Adv. Catal. 36 (1989) 55–172, https://doi.org/10.1016/S0360-0564(08)60017-6.
[44] R. van den Berg, G. Prieto, G. Korpershoek, L.I. van der Wal, A.J. van Bunningen, S. Lægsgaard-Jørgensen, P.E. de Jongh, K.P. de Jong, Structure sensitivity of Cu and CuZn catalysts relevant to industrial methanol synthesis, Nat. Commun. 7 (2016) 1–7, https://doi.org/10.1038/ncomms13057.
[45] J.L. Eslava, E. Gallegos-Suárez, A. Guerrero-Ruiz, I. Rodríguez-Ramos, Effect of Mo promotion on the activity and selectivity of Ru/Graphite catalysts for Fischer-Tropsch synthesis, Catal. Today 357 (2020) 185–192, https://doi.org/10.1016/j.cattod.2019.05.051.
[46] J. Bian, M. Xiao, S. Wang, X. Wang, Y. Lu, Y. Meng, Highly effective synthesis of dimethyl carbonate from methanol and carbon dioxide using a novel copper–nickel/graphite bimetallic nanocomposite catalyst, Chem. Eng. J. 147 (2-3) (2009) 287–296, https://doi.org/10.1016/j.cej.2008.11.006.
[47] G. Prieto, J. Zečević, H. Friedrich, K.P. de Jong, P.E. de Jongh, Towards stable catalysts by controlling collective properties of supported metal nanoparticles, Nat. Mater. 12 (1) (2013) 34–39, https://doi.org/10.1038/nmat3471.
[48] C.E. Pompe, M. Slagter, P.E. de Jongh, K.P. de Jong, Impact of heterogeneities in silica-supported copper catalysts on their stability for methanol synthesis, J. Catal. 365 (2018) 1–9, https://doi.org/10.1016/j.jcat.2018.06.014.
[49] X. Dong, H.-B. Zhang, G.-D. Lin, Y.-Z. Yuan, K.R. Tsai, Highly active CNT-promoted $Cu-ZnO-Al_2O_3$ catalyst for methanol synthesis from $H_2/CO/CO_2$, Catal. Lett. 85 (2003) 237–246, https://doi.org/10.1023/A:1022158116871.
[50] M. Che, O. Clause, C. Marcilly, Preparation of solid catalysts: Supported catalysts: Deposition of active component: Impregnation and ion exchange, in: G. Ertl, H. Knözinger, J. Weitkamp (Eds.), Handbook of Heterogeneous Catalysis, VCH Verlagsgesellschaft mbH, Weinheim, Germany, 1997, pp. 191–207, https://doi.org/10.1002/9783527619474.ch2b.
[51] M. Thommes, K. Kaneko, A.V. Neimark, J.P. Olivier, F. Rodriguez-Reinoso, J. Rouquerol, K.S.W. Sing, Physisorption of gases, with special reference to the evaluation of surface area and pore size distribution (IUPAC Technical Report), Pure Appl. Chem. 87 (2015) 1051–1069, https://doi.org/10.1515/pac-2014-1117.
[52] C.M. van den Bleek, K. van der Wiele, P.J. van den Berg, The effect of dilution on the degree of conversion in fixed bed catalytic reactors, Chem. Eng. Sci. 24 (4) (1969) 681–694, https://doi.org/10.1016/0009-2509(69)80061-8.
[53] P. Munnik, P.E. de Jongh, K.P. de Jong, Recent developments in the synthesis of supported catalysts, Chem. Rev. 115 (14) (2015) 6687–6718, https://doi.org/10.1021/cr500486u.
[54] M. Nunes, D.M. Fernandes, M.V. Morales, I. Rodríguez-Ramos, A. Guerrero-Ruiz, C. Freire, Cu and Pd nanoparticles supported on a graphitic carbon material as bifunctional HER/ORR electrocatalysts, Catal. Today (2019), https://doi.org/10.1016/j.cattod.2019.04.043.
[55] M.R. Cuervo, E. Asedegbega-Nieto, E. Díaz, S. Ordóñez, A. Vega, A. Belén Dongil, I. Rodríguez-Ramos, Modification of the adsorption properties of high surface area graphites by oxygen functional groups, Carbon 46 (15) (2008) 2096–2106, https://doi.org/10.1016/j.carbon.2008.08.025.
[56] M. d'Halluin, T. Mabit, N. Fairley, V. Fernandez, M.B. Gawande, E. Le Grognec, F.-X. Felpin, Graphite-supported ultra-small copper nanoparticles – Preparation, characterization and catalysis applications, Carbon 93 (2015) 974–983, https://doi.org/10.1016/j.carbon.2015.06.017.
[57] I. Robinson, R. Harder, Coherent X-ray diffraction imaging of strain at the nanoscale, Nat. Mater. 8 (4) (2009) 291–298, https://doi.org/10.1038/nmat2400.
[58] K.D.M. Harris, M. Tremayne, B.M. Kariuki, Contemporary advances in the use of powder X-ray diffraction for structure determination, Angew. Chem. Int. Ed. 40 (2001) 1626–1651, https://doi.org/10.1002/1521-3773(20010504)40:9<1626::AID-ANIE16260>3.0.CO;2-7.

[59] T. Lunkenbein, J. Schumann, M. Behrens, R. Schlögl, M.G. Willinger, Formation of a ZnO overlayer in industrial $Cu/ZnO/Al_2O_3$ catalysts induced by strong metal-support interactions, Angew. Chem. Int. Ed. 54 (15) (2015) 4544–4548, https://doi.org/10.1002/anie.201411581.
[60] Roine A., Lamberg P., Mansikka-aho J., Björklund P., Kentala J.-P., Talonen T., Kotiranta T., Ahlberg R., Gröhn A., Saarinen O., Myyri J., Sipilä J., Vartiainen A., Outotec's HSC Chemistry software, version 7, (2011).
[61] V. Dieterich, A. Buttler, A. Hanel, H. Spliethoff, S. Fendt, Power-to-liquid via synthesis of methanol, DME or Fischer–Tropsch-fuels: A review, Energy Environ. Sci. 13 (10) (2020) 3207–3252, https://doi.org/10.1039/d0ee01187h.
[62] J. Xie, H.M. Torres Galvis, A.C.J. Koeken, A. Kirilin, A. Iulian Dugulan, M. Ruitenbeek, K.P. de Jong, Size and promoter effects on stability of carbon-nanofiber-supported iron-based Fischer–Tropsch catalysts, ACS Catal. 6 (6) (2016) 4017–4024, https://doi.org/10.1021/acscatal.6b00321.
[63] M.S. Spencer, The role of zinc oxide in Cu/ZnO catalysts for methanol synthesis and the water-gas shift reaction, Top. Catal. 8 (1999) 259–266, https://doi.org/10.1023/A:1019181715731.
[64] C. Wöll, The chemistry and physics of zinc oxide surfaces, Prog. Surf. Sci. 82 (2-3) (2007) 55–120, https://doi.org/10.1016/j.progsurf.2006.12.002.
[65] O.V. Larina, P.I. Kyriienko, D.Y. Balakin, M. Vorokhta, I. Khalakhan, Y.M. Nychiporuk, V. Matolín, S.O. Soloviev, S.M. Orlyk, Effect of ZnO on acid–base properties and catalytic performances of ZnO/ZrO_2–SiO_2 catalysts in 1,3-butadiene production from ethanol–water mixture, Catal. Sci. Technol. 9 (15) (2019) 3964–3978, https://doi.org/10.1039/c9cy00991d.
[66] M. Kurtz, J. Strunk, O. Hinrichsen, M. Muhler, K. Fink, B. Meyer, C. Wöll, Active sites on oxide surfaces: ZnO-catalyzed synthesis of methanol from CO and H_2, Angew. Chem. Int. Ed. 44 (18) (2005) 2790–2794, https://doi.org/10.1002/anie.200462374.
[67] G. Prieto, M. Shakeri, K.P. de Jong, P.E. de Jongh, Quantitative relationship between support porosity and the stability of pore-confined metal nanoparticles studied on $CuZnO/SiO_2$ methanol synthesis catalysts, ACS Nano 8 (3) (2014) 2522–2531, https://doi.org/10.1021/nn406119j.
[68] C.E. Pompe, D.L. van Uunen, L.I. van der Wal, J.E.S. van der Hoeven, K.P. de Jong, P.E. de Jongh, Stability of mesocellular foam supported copper catalysts for methanol synthesis, Catal. Today 334 (2019) 79–89, https://doi.org/10.1016/j.cattod.2019.01.053.